OSJI OPEN SCIENCE JOURNAL

RESEARCH ARTICLE

Development of Modified Sliding Mode Control of the LCC Series – Parallel Resonant Converter based on Frequency Variation

James Halivor[1*], Feng Ying[1]

[1]South China University of Technology, Guangzhou, China

*Corresponding author: James Halivor: jayjunior72@ymail.com

OPEN ACCESS

Citation: Halivor J., Ying F. (2023) Development of Modified Sliding Mode Control of the LCC Series – Parallel Resonant Converter based on Frequency Variation. Open Science Journal 8(2)

Received: 8th October 2022

Accepted: 23rd January 2023

Published: 6th October 2023

Funding: The author(s) received no specific funding for this work

Competing Interests: The authors have declared that no competing interests exists.

Abstract:

This paper delves into the components of high-frequency power supplies and high voltages, both of which see extensive use in fields such as high voltage applications, industrial applications, atmospheric pressure plasma processing, X-ray high voltage applications, electrostatic precipitation, and so on. To counteract these undesirable consequences of converter operation, the LCC criteria provide a trustworthy choice by including a topology that makes optimal use of leakage inductance and convoluting capacitance. Because of these benefits, it can be used for a wide variety of power and energy tasks. With the LCC Series-Parallel Resonant Converter, you get the benefits of both the parallel and series resonant converters. This includes lower peak currents, smaller switching frequency changes, and more efficiency. For a limited class of nonlinear systems, the Sliding Mode Control (SMC) approach provides sufficient robust control. The converter's topology can be uneven, but the sliding mode method can ignore that. Signal-based Motion Control (SMC) maps signal routes onto a surface (the sliding surface or hyperplane). Points on a trajectory can be guided by an external control signal along a sliding surface (or hyperplane). For the purposes of this paper, a current-mode control scheme is used. Sliding mode controller with a strong amplitude modulation setup. Due to the non-linearities seen in both simulation and experimental data, small-signal modelling was performed to equalize and theoretically determine the system characteristics.

Keywords: LCC series-parallel resonant converter, Current-mode control, Robust algorithm, Frequency variation.

Introduction

Resonant converters have several advantages over standard Pulse-Width-Modulation (PWM) converters, including the ability to switch at higher frequencies while still contributing significantly to the power conversion process. Zero Current Switching (ZCS) and Zero Voltage Switching (ZVS) conditions can be obtained to reduce switching losses which arise from the on and off states of the switches through the management of the resonant converter energy by adjusting its operating frequency and regulating conditions of input power to achieve desired voltage [1]. This is the main advantage. In addition to its benefits, it can also reduce Electromagnetic Interference (EMI) [2] and smooth out switching transactions, both of which help lower the noise emanating from converter parts.

Good voltage accumulation and correct open and short-circuit characteristics are made possible by the LCC series-parallel resonant converter [3,4], which implements and sums up the advantage of both the series resonant converter (SRC) and the Parallel Resonant Converter (PRC). Components of the LCC-SPRC typically include a resonant capacitor Cs and an inductor Ls connected in series and parallel with a capacitor Cp. The development of the power transfer mechanism relies heavily on the modelling and control of the LCC series-parallel resonant converter to boost the output performance. Several small-signal models for steady-state operation of the LCC series-parallel resonant converter have been produced in the literature [5] to investigate the converter's intrinsic properties; the findings from these models can be incorporated into the controller design [6].

To keep ZVS or ZCS conditions in high-voltage application ranges, the soft-switching strategies for the LCC series-parallel resonant converter typically involve discussing some phase-shift modulation control or frequencies-shift modulation control methods [7]. When dealing with significant load changes, a close-loop control strategy using the output voltage as the control input signal is necessary to increase the transient response.

This study discusses a modified Sliding Mode Control (SMC) strategy for the LCC-SPRC algorithm based on the modelling method. SMC method is a typical algorithm for robust control, and it may sustain dynamic response while retaining robustness against load and input voltage fluctuations. [18,19] By perturbing and linearizing the average model of the LCC Series-Parallel Resonant Converter, an appropriate small-signal model is produced. A precise operation point leads to a modest ripple approximation. Certain control approaches were applied in systems with variable structures, and they were later adapted for use in DC-DC converters [8,9].

Based on the typical SMC technique, a modified SMC for the LCC series-parallel resonant converter is discussed in this study. By selecting a particular industrial application module, the operating principle of the LCC series-parallel resonant converter is investigated, and the state space small-signal analysis is provided for use in the design of the state control. The output performance is guaranteed by the SMC algorithm when the voltage is used as the feedback signal.

The structure of this document is as follows: Section 2 introduces the operating principles of the LCC series-parallel resonant converter. In Section 3, the state space small-signal analysis of the LCC series-parallel resonant converter is explored, and in Section 4, the design approach is outlined. Section 5 provides simulation data to demonstrate the effectiveness of the proposed strategy. The final portion concludes the study presented in this paper.

Principle of operation

LCC module circuit and parameters

The main LCC-SPRC module prototype used in this work is shown in Figure 1, and the main topology of LCC-SPRC is given in Figure 2. It is made of electronic components of 4 IGBTs S1˜S4, and four (4) anti-diodes D1˜D4. The main constituents of the resonant tank include the capacitor Cs, the inductor Ls in series, and another capacitor, Cp. Leakage inductance and capacitance are requisite features of the high voltage transformer and with it comes the derivatives of both primary and secondary ends Ls prone to transformer conversions. Four secondary rectifier diodes, DR1˜DR4. C_o and L_o are the output filtering capacitance and inductance respectively. Ro is the load with the voltage across it, and the output voltage is V_o.

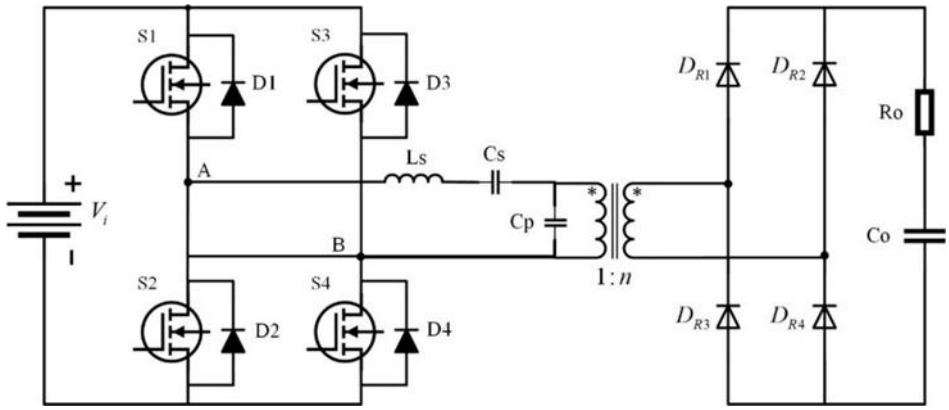

Figure 1. The main circuit of LCC-SPRC (Series-Parallel Resonant Converter)

Table 1: Specifications of LCC Converter

Parameter Specification	Parameter Value	Parameter Specification	Parameter Value
Input Voltage, V_{in}	200~400V	Transformer turns ratio. (Np: Ns)	5:1
Output Voltage, V_{out}	48V	Dead Time, t_d	400nS
Output Power, P_o	100~500W	Capacitance, C_{ds}	200pF
Minimum Switching Frequency, f_{min}	100kHz	Parallel Capacitance, C_p	20nF
Series Parallel Frequency, f_{spr}	100kHz	Filter Inductor, L_f	400µH
Series Capacitance, C_s	20nF	Filtering Capacitor, C_f	470 µF
Resonant Tank Inductor, L_r	252µH		

The primary circuit description of the prototype consists of two boards (power and control). The function-containing chips can provide high-level analogue integration, and the inbuilt voltage regulator makes single-rail operation and dual-

edge control possible (frequency modulation). The Low Dropout (LDO) regulator combines ultra-low current consumption with the high performance demanded by Radio Frequency (RF) and precision analogue applications. The circuit board for sliding mode control of the LCC resonant converter can be designed to operate at different voltages and power levels.

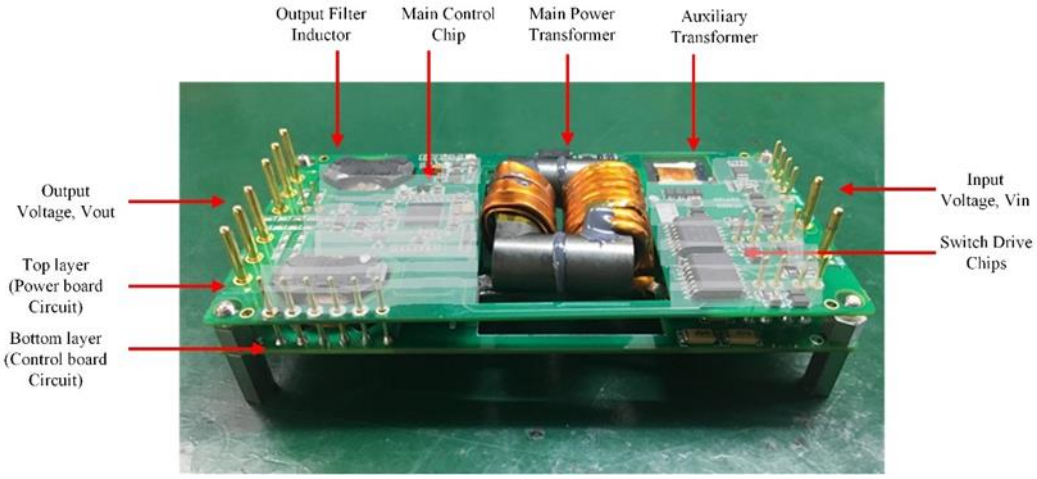

Figure 2. Photo of Circuit Prototype

The steady-state solution is rightly dependent on the operating point of the system (desired output) and the results can be obtained via computation. The control input, u_1(Duty Cycle), u_2 (Switching frequency to the output voltage). The Low Dropout (LDO) regulator satisfies the need for great performance in RF and precision analogue applications while drawing very little current. This LCC resonant converter sliding mode control circuit board, however, may be set up to work with a wide range of input and output voltages and power densities.

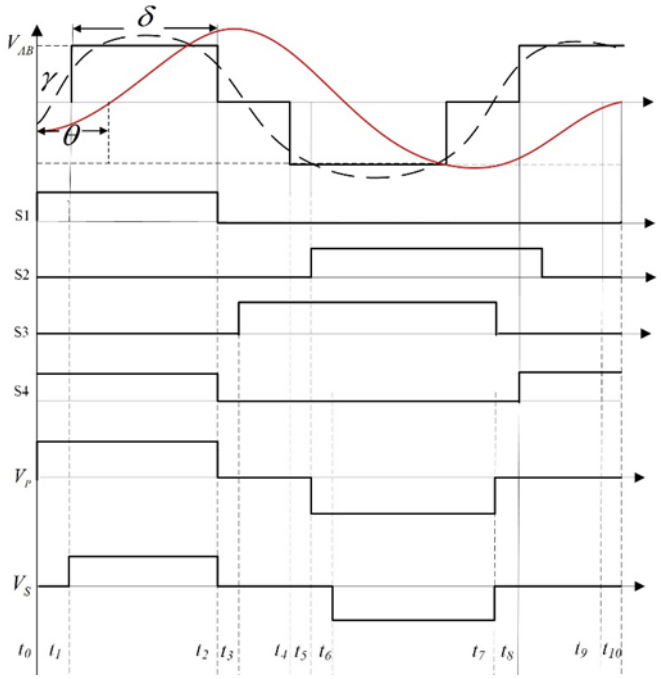

Figure 3. Key waveforms of the DC-DC Resonant Converter.

As shown in Fig 3, the conduction angle suffices by varying an angle "δ", the pulse-width "θ" controls the waveform V_{AB}. The signals that gate switches S2 & S4 are reduced in duration by an angle "θ" and added to the gating signals for S1 and S3. Thus, the rising edges of the gating signals for S1 and S2 are aligned, whereas the falling edges of the gating signals for S3 and S4 align [10].

LCC converter modes of operation

The basic circuit diagram of the LCC-type SPRC with an inductive output filter is shown in Fig 1. A careful look at circuit parameters, operations and some useful applications is explained in this section.

Mode 1 (t_0~t_1)

In the event of to, the current, i_{Ls} maps to a blank value and the V_{CS}, voltage of this series capacitor C_s, is negative. Switches S1 and S4 are turned on with ZVS. Inductor current i_{L5} begins to rise from zero, flowing through S1, C_s, L_s, T_r and S4. Diodes D_{R1} and D_{R4} are turned-on. The capacitive voltage, V_{Cp} of the parallel resonant capacitor, C_p negotiates with V_o /n by the output voltage. The presumed quantities show V_o as the output voltage, the turns ratio, n. Then at t1 resonant current, i_{Ls} go to zero, and D_{R1} and D_{R4} are turned off, the equivalent circuit is shown above in Fig 4.

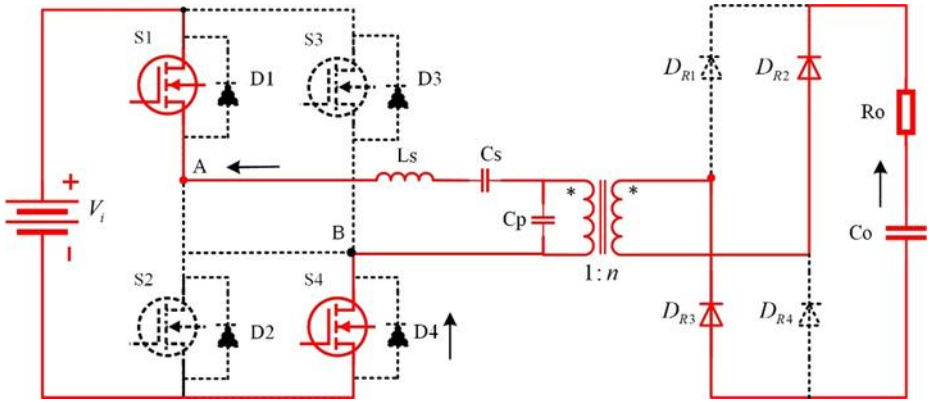

Figure 4. LCC-SPRC Switch Mode 1

Mode 2 (t_1~t_2)

During t_1, the current i_{Ls} after it becomes negative D4 and D1 are turned on, and the terminal voltage of S4 and S1 is regulated to zero. To achieve zero voltage, switches S4 and S1 are switched on and in a very prevalent routine. The resonant voltage, V_{cp} gradually reduces from V_o/n as the parallel capacitor, C_p discharges. For the DC bus to harbor any form of energy it is likely to go through energy storage components C_s, L_s, and C_p at this time all the secondary rectifier diodes are turned off, and the resonant converter stops transmitting energy to the secondary side of T_r. The load energy is provided by the output filter capacitor, the equivalent circuit is depicted in Fig 5.

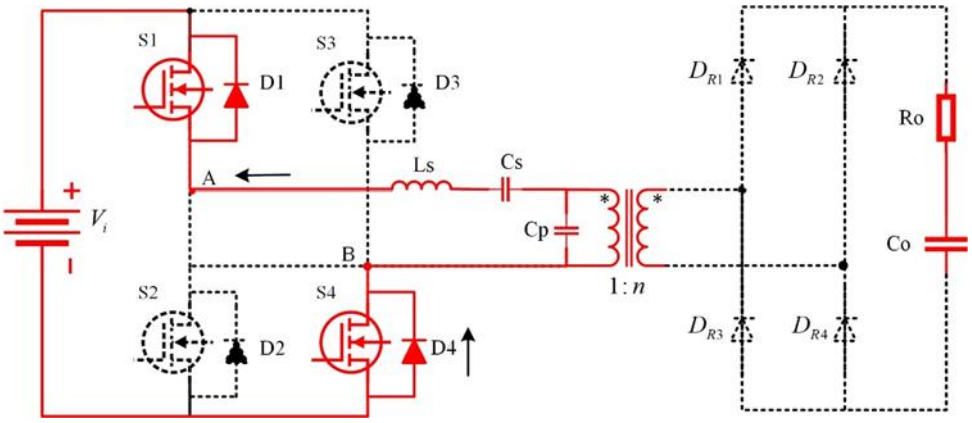

Figure 5. LCC-SPRC Switch Mode 2

Mode 3 (t_2~t_3)

During this switch mode, V_{Cp} can be evaluated as negative with V_o/n. Secondary diodes D_{R2} and D_{R3} are turned on, V_{Cp} of C_p is clamped to V_o/n by the output voltage. The resonant inductor current, i_{Ls} is negative, flowing through D4, C_s, L_s, T_r and D1. Transmitted energy on the less primary side is stored energy and transmitted to the DC bus. At t_3, the resonant inductor current is zero, D_{R2} and D_{R3} are turned-off with zero-current switching.

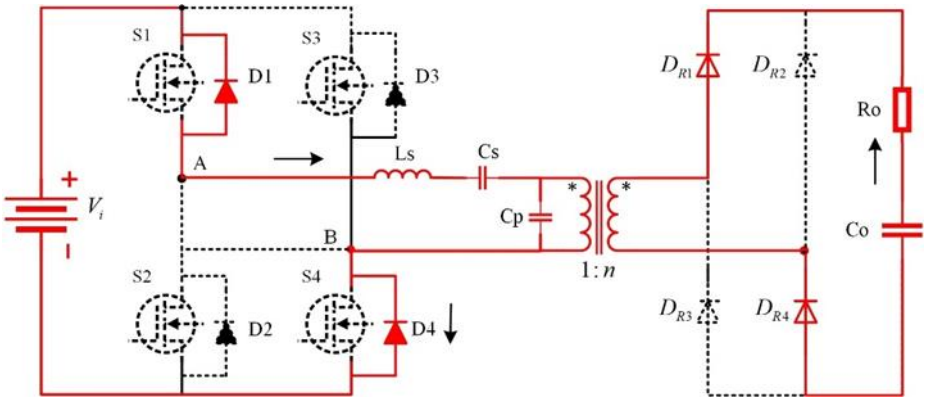

Figure 6. LCC-SPRC Switch Mode 3

Mode 4 (t_3~t_4)

This mode represents the first half of the converter switch cycle, all the diodes and IGBTs are turned off, i_{Ls} goes to zero, Voltages V_{Cs} and V_{Cp} are constant, and the load energy is provided by the output filter capacitor.

2nd half-Mode (t_5~t_{10})

At t_4, switches S2 and S3 realize zero-current switching, and then LCC-SPRC's working condition in the second half cycle is similar to the conditions that have been illustrated in the first-half cycle and hence completing the full cycle operating principle as illustrated in Fig. 7 below.

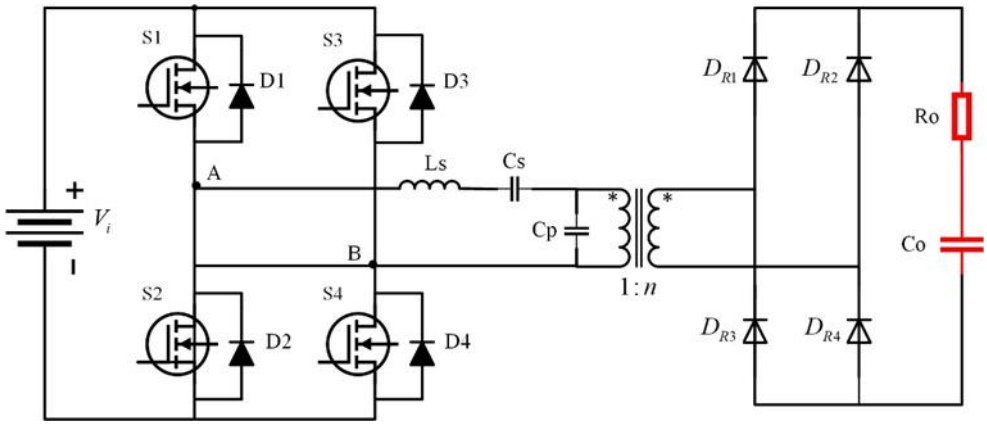

Figure 7. LCC-SPRC Switch Mode 4

State space small-signal analysis

As shown in Fig. 8, the state equations (1), (2) and (3) of the power stage are as follows:

Series and parallel inductance and capacitance:

$$Li'_{LS}(t) = -V_s + V_{AB} - V_P \tag{1}$$

$$C_s V'_{CS}(t) = i_{LS}(t) \tag{2}$$

$$C_p V'_{Cp}(t) + \mathrm{sgn}(V_{Cp}) i_{Lf} = i_{Ls}(t) \tag{3}$$

Solving and evaluating output differentials

$$L_f i'_{lf} + e'_{sr}\left[i_{lf} + i_o\right] + V_{Cf}\left[\frac{R_L - e'_{sr}}{R_L}\right] = \left|V_{Cp}\right| \tag{4}$$

The factor, $[i_{lf}+, i_o\,]$ from equation (4) can be mathematically deduced as:

$$\left[i_{lf} + i_o\right] = C_f V'_{Cf}\frac{e_{sr}}{e'_{sr}} + \frac{V_{Cf}}{R_L} \tag{5}$$

The Output voltage variables in equation (6) considering the input current (source current) in equation (7)

$$V'_{output} = V_{Filter} + V_{Cfilter} + V_{OutputFilter} \tag{6}$$

$$i_{Input} = \frac{1}{T_S}\int_0^{T_S} i_{Ls}\frac{V_{AB}(t)}{V_{in}}dt \tag{7}$$

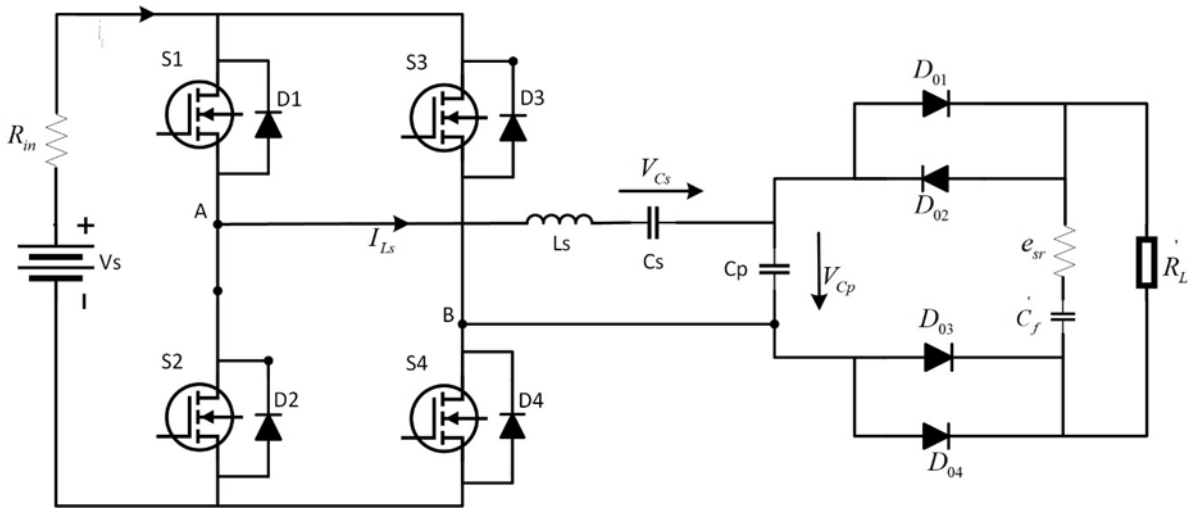

Figure 8. The Equivalent Circuit of the LCC-SPRC.

The state vector obtained from the above presumptions is given by:

$$x(t) = \left[i_{Ls}(t) \quad V_{Cs}(t) \quad V_{Out}(t) \right]^T \tag{8}$$

Linearization and perturbation

The new state variables upon employing the averaging method are open-angle $\langle i_{Ls} \rangle_1$, $\langle V_{Cs} \rangle_1 \text{and} \langle V'_{Out} \rangle_0$. By separating into real (R) and imaginary parts (q) and assigning Complex Fourier Co-efficients (CFC), the following is deduced:

$$\langle V_{AB} \rangle_1 = \frac{V_{in}}{\pi} \left[\sin(\pi D) + j(\cos(\pi D) - 1) \right] \tag{9}$$

Thus, the complex Fourier components in equation (10) takes care of the added circuit disturbances, and the equation inculcates all the voltage parameters necessary to compute the real and imaginary parts of the system steady-state analysis explained in equation (11)-(15).

$$CFC \begin{cases} \langle i_{Ls} \rangle_1 = i_{LsR} + i_{Lsq} = a_1 + jb_1 \\ \langle V'_{Out} \rangle_0 = V'_{Out} = a_4 \\ \langle V_{Cs} \rangle_1 = V_{CsR} + V_{Csq} = a_2 + jb_2 \\ \langle V_{Cp} \rangle_1 = V_{CpR} + V_{Cpq} = a_3 + jb_3 \end{cases} \tag{10}$$

Real and imaginary parts from the equation

$$\frac{da_1}{dt} = \omega_s b_1 - \frac{a_2}{L_s} - \frac{a_3}{L_s} + \frac{V_{in}}{L_s} \sin(\pi D) \tag{11}$$

$$\frac{da_2}{dt} = \omega_s b_2 + \frac{a_1}{C_s} \tag{12}$$

$$\frac{db_1}{dt} = -\omega_s a_1 - \frac{b_2}{L_s} - \frac{b_3}{L_s} + \frac{V_{in}}{\pi L_s} [\cos(\pi D) - 1] \tag{13}$$

$$\frac{db_2}{dt} = -\omega_s a_2 + \frac{b_1}{C_s} \tag{14}$$

$$\frac{da_4}{dt} = \frac{1}{C'_f} . \frac{2\sqrt{a_1^2 + b_1^2}}{\pi} . [1 - \cos(\theta)] - \frac{V'_{Out}}{C'_f R'_L} \tag{15}$$

Finally, the above equations (9)-(15) can be re-written considering the derivations as

$$abs(i_{Lf})_1 = \frac{2\left|\sqrt{a_1^{\,2} + b_1^{\,2}}\right|}{\pi}.[1-\cos(\theta)] \tag{16}$$

$$\theta = \cos^{-1}\left(\frac{\omega_s C_p a_4}{2\sqrt{a_1^{\,2} + b_1^{\,2}}} - 1\right) \tag{17}$$

Voltage inscribed on the parallel capacitor is not considered as a state variable so the terms of open-angle$\langle i_{Ls}\rangle_1$ and $\langle V_{Cs}\rangle_1$ as a_3 and b_3 in:

$$a_3 = \frac{1}{C_p \omega_s \pi}[a_1\beta + b_1\varphi] \qquad \beta = \sin^2(\theta)$$

$$b_3 = \frac{1}{C_p \omega_s \pi}[b_1\beta - a_1\varphi] \qquad \varphi = \pi + \frac{1}{2}\sin(2\theta) - \theta$$

The duty cycle is D and ω_s is the switching frequency which each represent the control inputs u_1 and u_2 respectively. The amplitudes of the voltages in the resonant tank and output are as follows:

$$\begin{aligned} y_1 &= a_4 \\ y_2 &= 2.\sqrt{a_1^{\,2} + b_1^{\,2}} \\ y_3 &= 2.\sqrt{a_2^{\,2} + b_2^{\,2}} \end{aligned} \tag{18}$$

The small signal analysis of the LCC SPRC is evidently obtained by equating the derivatives of equations to zero and evaluating the steady-state value of the angle θ. Therefore, the steady-state solutions of the equations with subscript 'ss' are given by:

$$a_{1ss} = R\sin(\pi D) - \frac{b_{1ss}}{Z} \qquad a_{2ss} = \frac{b_{1ss}}{C_s.\omega_{s_{ss}}} \qquad b_{1ss} = \frac{R.Z^2}{(1+Z^2)}\left\{[\cos(D\pi)-1] + \frac{\sin(D\pi)}{Z}\right\}$$

$$b_{2ss} = -\frac{a_{1ss}}{C_s.\omega_{s_{ss}}} \qquad b_{3ss} = \frac{1}{\pi\omega_{s_{ss}} C_p}[b_{1ss}\beta_{ss} - a_{1ss}\varphi_{ss}] \qquad a_{3ss} = \frac{1}{\pi\omega_{s_{ss}} C_p}[a_{1ss}\beta_{ss} - b_{1ss}\varphi_{ss}]$$

$$a_{4ss} = \frac{R'_L\sqrt{a_{1ss}^{\,2} + b_{1ss}^{\,2}}}{\pi}[\cos(\theta_{ss})]$$

$$\varphi_{ss} = \pi + \frac{1}{2}\sin(2\theta_{ss}) - \theta_{ss} \qquad \beta_{ss} = \sin^2(\theta_{ss}) \qquad \theta_{ss} = 2.\tan^{-1}\sqrt{\frac{2\pi}{\omega_s C_p R'_L}}$$

$$Z = \frac{\beta_{ss}}{\varphi_{ss} - \pi\omega_{s_{ss}}^{\,2}.C_p L_s + \lambda\pi}$$

$$R = \frac{V_{in}.C_p.\omega_{s_{ss}}}{\beta_{ss}} \quad \text{and} \quad \lambda = \frac{C_p}{C_s}$$

To derive the requisite small-signal transfer function of desired output and input to produce a model of this form, there is the need for linearization. Thus, we have:

$$\begin{cases} \overrightarrow{\Delta\dot{a}} = E\overrightarrow{\Delta a} + F\overrightarrow{\Delta u} \\ \overrightarrow{\Delta y} = G\overrightarrow{\Delta a} + H\overrightarrow{\Delta u} \end{cases} \tag{19}$$

Where $\vec{a}$ represents the state vector, $\vec{u}$ is the input vector, Δ represent the respective minor-scale changes in parameter values and $\vec{y}$ is the output vector. The matrices of the system are described in E, F, G and H. The complex analytical linearization equations and system parameters are presented in [11] 'Ying F., Halivor J., (2019', a thesis compilation of the sliding mode parameters for the DC-DC converter.

Modified SMC control design

Sliding mode control method

The main idea illustrated here shows that this control system selects the adequate parameters of each structure and describes them to a preferred switching mechanism. The structures put across have been laid in these papers: 'Jeronimo J. (2015), Tan, X., Ruan, X., (2016), Abdelhédi, F., & Derbel, N. (2019)'. [12-14], they outline the system control designs that output stable control mechanisms. These structures are usually asymptotical and are either stable or unstable. An asymptotically stable system may consist of two structures. These structures are unique. The concept created by sliding mode is to create and develop paths that are dissimilar and non-inherent from its structures. This trajectory obtained from these structures shows a novella kind of motion known as the "Sliding Mode".

Taking into consideration its asymptotic unstable structure, a sliding mode behavior can be integrated to create a new trajectory or path. Let's consider the basic system of the characteristics of variable structure control technique in equation (20). The general equations are:

$$\begin{cases} \dot{x}_a = x_b \\ \dot{x}_b = m - Pux_a \end{cases} \tag{20}$$

Existence condition

Considering the basic scalar control system in equation (21), can be calculated as:

$$\dot{x} = S_f(x,t,u) \tag{21}$$

Where S_f and x are function vectors and column vectors respectively, u is the control input. This function equation is per the switching boundary representative points moving on the sliding surface, shown as $\xi(x,t)=0$ .Thus, we can have:

$$S_f(x,t,u) = \begin{cases} S_f{}^{+}(x,t,u^{+}) \\ S_f{}^{-}(x,t,u^{-}) \end{cases} \tag{22}$$

Hence, for sliding mode to exist, the phase trajectories of the two substructures (be it stable or unstable) shown in equation (22) must be co-existent with the vector function values $\xi(x,t)=0$. That is, when $\xi>0$, the equivalent state vector Sf+, must move in the direction of the sliding surface. The state vector components inscribed by 'n' conform to the sliding surface and should be represented as:

$$\begin{matrix} \lim_{\xi\to 0^{+}} S_{fn}{}^{+} < 0 \\ \lim_{\xi\to 0^{-}} S_{fn}{}^{-} > 0 \end{matrix} \Rightarrow \begin{matrix} \lim_{\xi\to 0^{+}} \nabla\xi.S_f{}^{+} < 0 \\ \lim_{\xi\to 0^{+}} \nabla\xi.S_f{}^{-} > 0 \end{matrix} \tag{23}$$

Then the differential implementation of equation (22) and (23) will be:

$$\frac{d\xi}{dt} = \sum_{i=a,b}^{n} \frac{\partial\xi}{\partial x_i}\frac{dx_i}{dt} = \nabla\xi.S_f \tag{24}$$

Therefore, the existence conditions for sliding mode from Equation (1) becomes:

$$\begin{matrix}\lim_{\xi\to 0^+}\frac{d\xi}{dt}<0\\ \lim_{\xi\to 0^-}\frac{d\xi}{dt}>0\end{matrix}\Rightarrow\lim_{\xi\to 0}\xi\frac{d\xi}{dt}<0 \tag{25}$$

Reaching conditions

It is sufficient to deduce that the reaching conditions should possess scalar discontinuous input, u

$$u=\begin{cases}u^+\to\xi(x)>0\\ u^-\to\xi(x)<0\end{cases} \tag{26}$$

The variable, x must be such that it is scaled [x+] and [x-] as shown in equation (27). It then relates the corresponding control inputs u+ and u-. The preamble for the reaching condition for sliding surface is denoted by:

$$\begin{matrix}[x^+]\in\xi(x)<0\\ [x^-]\in\xi(x)>0\end{matrix} \tag{27}$$

The steady state features of a substructure can be coupled with the field area and the other substructure in order to assure that the system RP will finally collide with the sliding surface.

SMC of the Series-Parallel Resonant Converter is introduced by the proposed control system and technique, which is compared to one proposed in [15] 'Castilla, M., Garcia de Vicuña, L., Lopez, M'. The paper states that it is essential to meet the control objectives, the most significant of which is voltage regulation. It is regulated to the reference voltage regardless of differences in power components and load changes. After this is activated, the second control objective can be implemented.

The second control purpose is to achieve a comparably high level of robustness under the same conditions of power constituent variations (aging, temperature fluctuations) to aid in the converter's continuous operation as resonant frequency. The last purpose of control is to provide rapid transient response despite load variations. The average dynamic model permits current-mode control; hence, 'current-mode control' is finished as the sliding line.' [16]. The configuration of the proposed controller is robust amplitude modulated. The loop outside is voltage-controlled and inner loop current-controlled. The following equations (28)-(31) depict the implemented controller:

$$S=i_{ref}-i_{inp} \tag{28}$$

$$i_{ref}=(k_o i_{out})+i_{\text{int}}+k_p(V_{ref}-V_{out}) \tag{29}$$

$$i_{\text{int}}=k_i\int(V_{ref}-V_{out})dt \tag{30}$$

$$k_o=\frac{V_{ref}}{V_{inp}} \tag{31}$$

With the inner current loop, we can keep up with the reference current required by the suggested sliding surface. The control input u acts on the flip-flop, Zero-Crossing Detector, and comparator to establish and synchronize the voltage across the resonating capacitor. The function of the feedback term is to ensure that the output voltage is equal to the reference voltage under steady-state conditions.[20] So, fix the unmodeled parasitic components. The modulator's ability to quickly react to changes in load is made possible by the feed-forward term, which aids it

in locating the appropriate control signal to maintain a constant voltage output. In conclusion, the modulator's overarching plan is to provide a stable functioning even when distortions are present by translating the synchronized control signal via logic circuits in order to automate and drive the power switches (S1-S4).

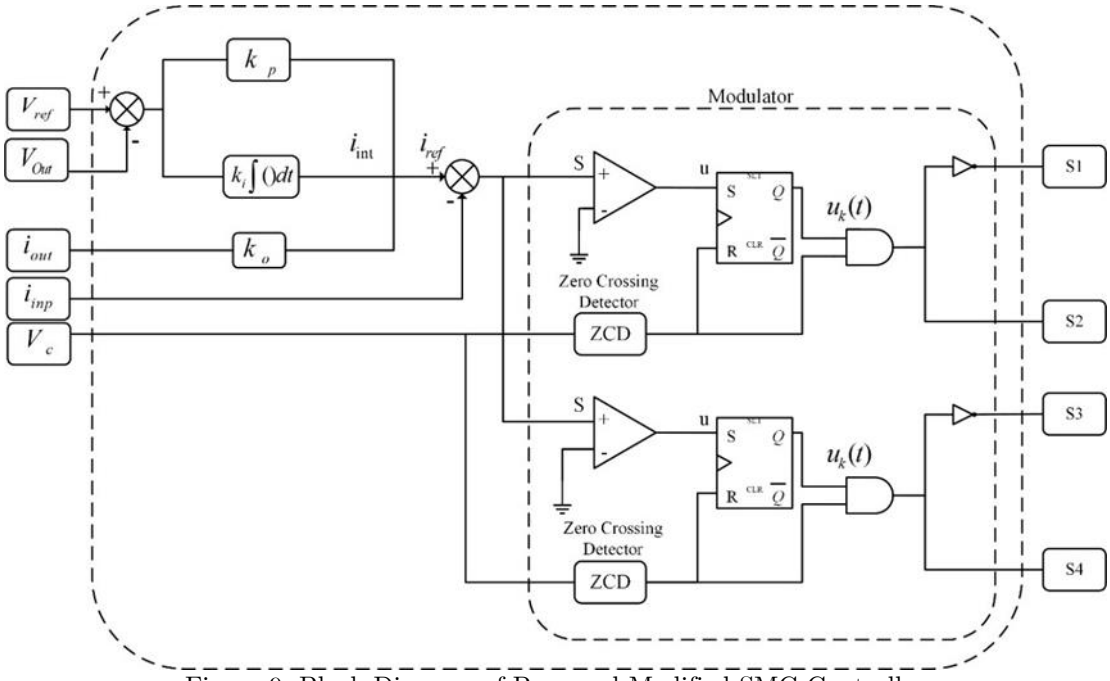

Figure 9. Block Diagram of Proposed Modified SMC Controller

SMC integration and development

This paper focused on the modelling and simulation of the LCC Series-Parallel Resonant Converter.As illustrated in Figure 10, the work involved utilizing of two simulation software interfaces.

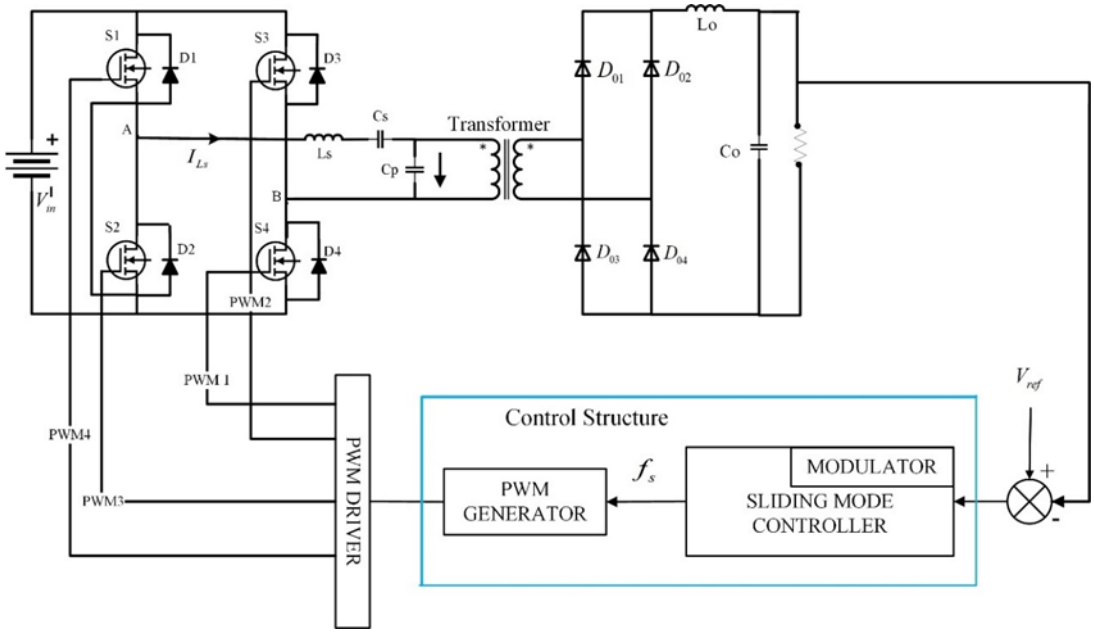

Figure 10. Flow Graph of LCC-SPRC Modified SMC Controller

Experimental Findings and Simulation were completed alongside Modelling, Design, Transfer Function Analysis, and Algorithm Derivation. Also, this helped immensely with confirming findings. The full-bridge diode rectifier was replaced by a Synchronous Rectifier, or SR, in an effort to improve the performance of LCC resonant converters. By using this method, MOSFETs can be used in place of diodes to detect current flow on the secondary side, allowing current to pass to the load.

Compared to an SR network, which allows power to flow in both directions of a circuit, diodes have significant drawbacks, including voltage dips and a single direction of circuit power flow [17]. The secondary side current is monitored and regulated by regulating the SR gate driving signals that cause these effects. The drain-source voltage (V_{Ds}) is measured, and the current is sensed via a current transformer. Even though there is an increase in circuit complexity and the need for extra compensating components, accuracy is reported to have increased in published works.[21,22] Algorithm flow diagram depicting simulated current and voltage waveforms in an SR network. Fig. 11. Linearizing the converter's small-signal model, computing the current-mode sliding surface to yield the desired voltage output [23], and visualizing the relevant transfer functions in relation to the control input, switching frequency, etc. are the foundations of design codes.

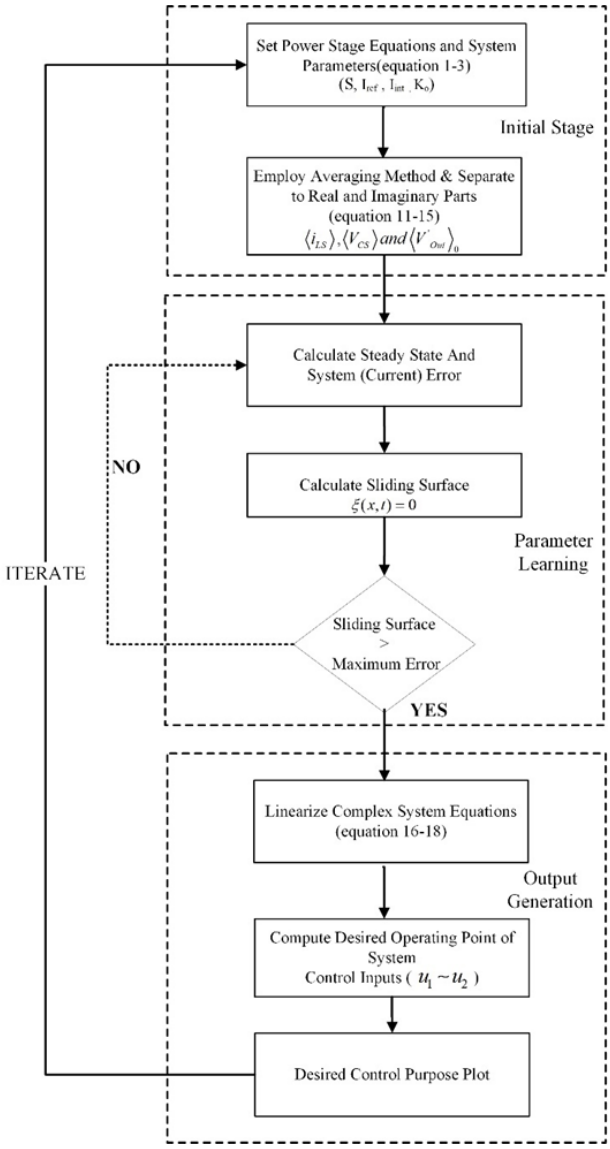

Figure 11. Robust Algorithm Flow Graph

Simulation and results

In order to achieve the desired voltage output and draw the required transfer functions in relation to the control input, switching frequency, etc., the design codes are based on a flowchart-like algorithm that linearizes the tiny signal model of the converter. The results of the simulation were obtained with the use of simulation software interfaces. The former is used to design, model, and simulate to obtain desired output and waveforms as well as for verification, while the latter is responsible for developing the algorithm in Figure 11 and Simulink models to obtain the suitable operating points of the system with its requisite plots and graphs. Figure 12 shows that the signals derived from the current and voltages are within acceptable ranges, and the currents have a sinusoidal shape. The system exhibits steady behavior when the nominal control parameters are used. As we can see from the FFT comparisons, the number of harmonics needed for precise results varies depending on the resonant converter setup, the ratio of switching frequency to resonance frequency, or the pulse width.

The output of the proposed converter is shown in Figures 14 and 15 to vary from 100% to 50% throughout a 100-500W load range, demonstrating its effectiveness under dynamically varying load conditions.

Half of the output voltage, or 100V, is applied as stress across the active switch. Five cases are studied in FFT in Figure 13 to confirm the effect of each control parameter.

It takes 1.5 seconds at 9A-12A to reach steady state. The desired 12A output current and 200V output voltage waveform is shown in Figure 15.

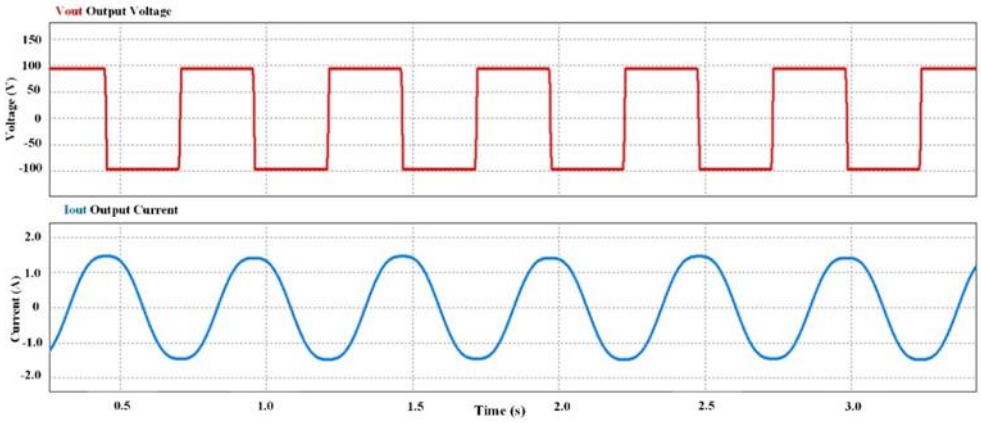

Figure 12. Simulation waveform of the LCC-SPRC converter under Input Voltage-200V, Reference Voltage-48V, 300W.

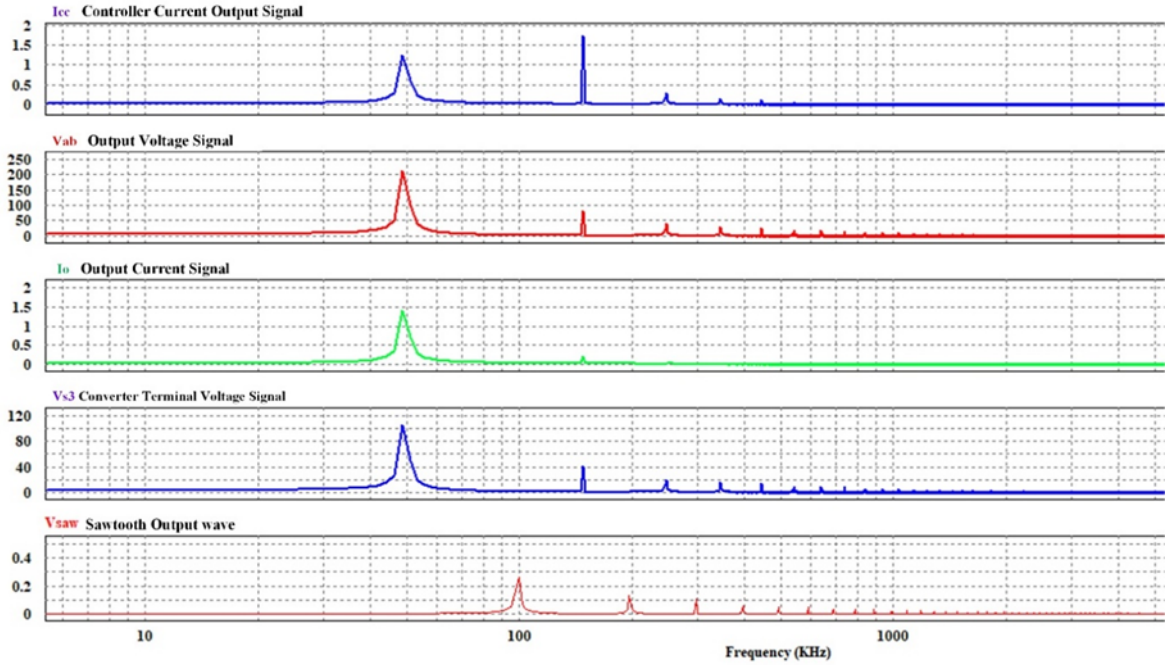

Figure 13. Key waveform (FFT) of the LCC-SPRC under proposed SMC controller.

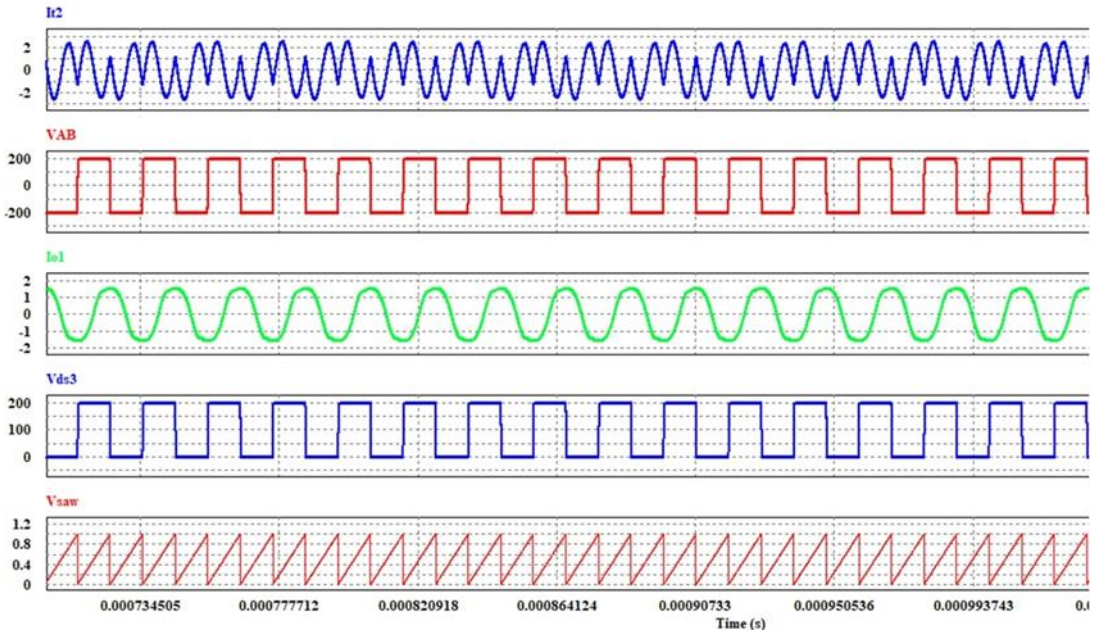

Figure 14. Key waveform (Time) of the LCC-SPRC under proposed SMC controller

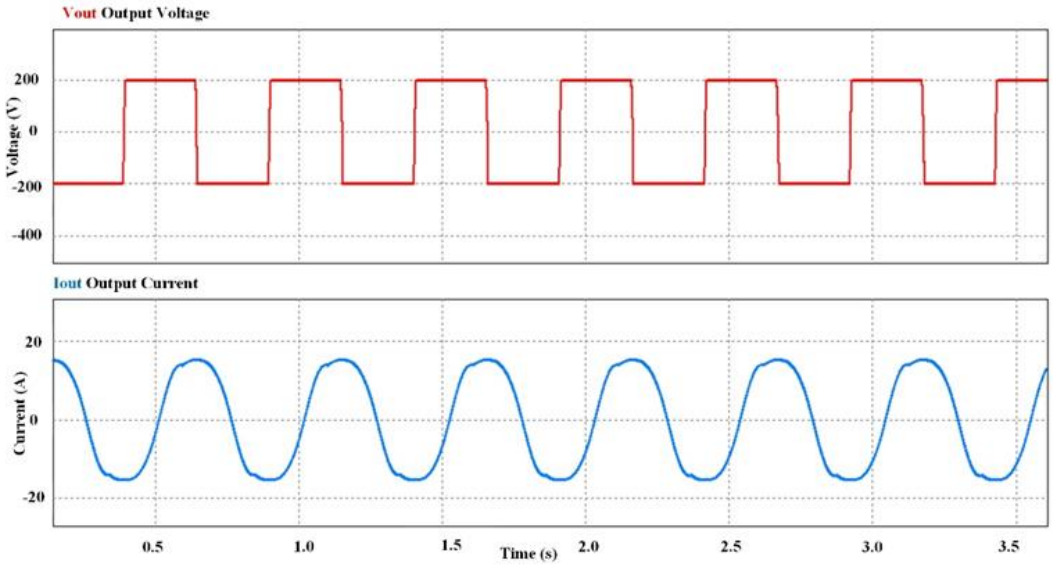

Figure 15. Simulation waveform of the LCC-SPRC converter under Input voltage-300V, Reference voltage-48V, 500W

Note that a varied range of responses can be obtained by changing the sliding surface parameter. Hence, the theoretical aspect of the proposed control scheme is verified by simulation. Figure 16 depicts the experimental circuit board for the LCC Resonant Converter's sliding mode control. This board is configurable for operation at various voltages and power levels.

Discussion

Evidence of this expansion of control measures may be found in the literature, which bodes well for the field's future. It's hardly shocking that the semi-conductor revolution and new mathematical ideas have stoked curiosity about this field of study. Within the scope of this control scheme, new methods for the design, analysis, and control of LCC resonant converters—in particular Sliding Mode Control—have been devised. The hunt and need for supercomputers has prompted widespread use of such converters in power conversion, which is the focus of the research presented in this thesis. In order to build a controller that will be helpful for this purpose, a linear approach was shown to be possible through the linearization of non-linear characteristics and the small-signal modeling of switch-mode power supplies.

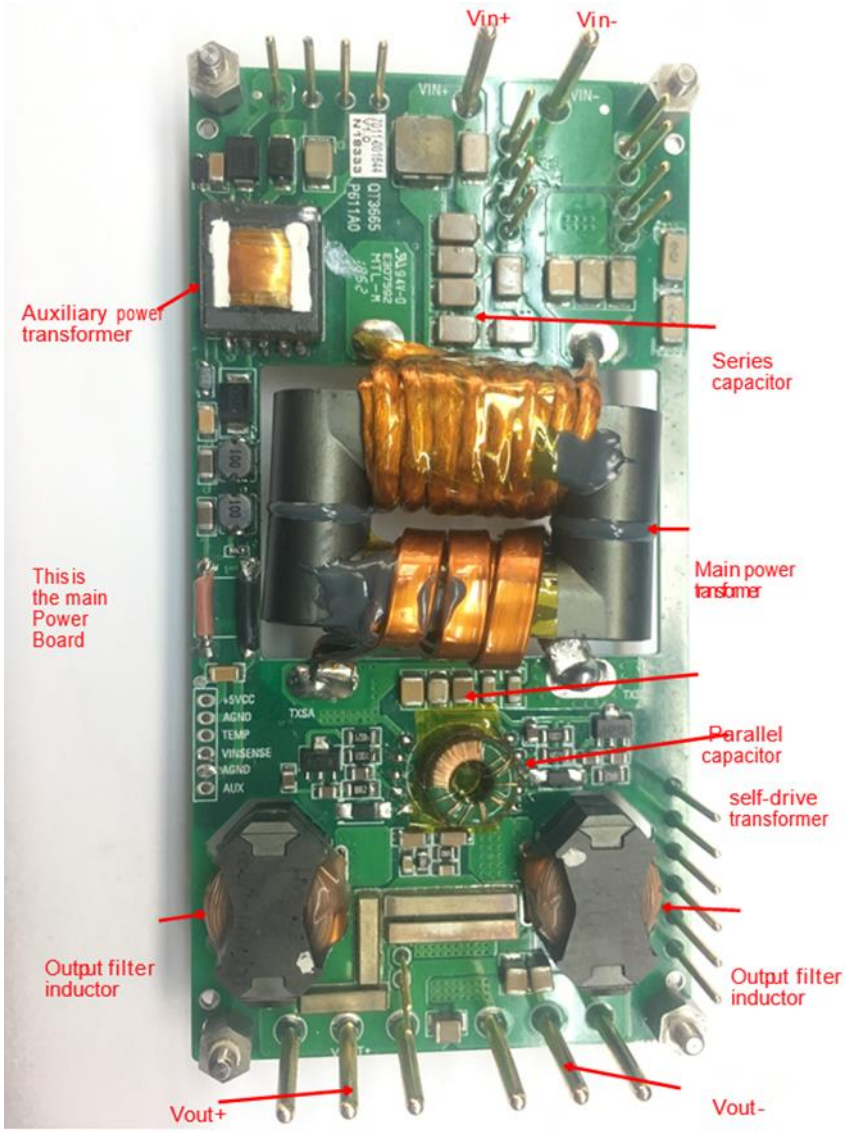

Figure 16 Labelled experimental circuit of the LCC resonant converter

Conclusion

In this study, a sliding-mode control for use with robust-amplitude modulation is developed with the goal of expanding the usefulness of DC-DC converters, specifically SPRCs. This work showcased the linearization of these non-linear factors and the adoption of a linear approach in controller design, both of which are necessary for the modelling of switch-mode power supply and small-signal modelling. In spite of its inherent robustness, the proposed control methodology may allow for a more thorough stability analysis of the sliding mode controller, opening the door to the use of additional system methods to achieve an even higher maximum perturbation parameter limit. Reduce harmonic distortions and experiment with different waveforms on the input characteristics using algorithms designed with complete access to all system states and developed with numerical analysis built in. When implemented together, the suggested controller and modulator create a system that is highly resilient to variations in load and power components.

The stability study of the sliding mode controller may be extended to include the use of other system methods to achieve a better upper bound on the perturbation parameter. It is possible to construct algorithms that perform numerical analysis and experiments based on these analyses, and it is also possible to design algorithms that have full access to all system states. Although this new controller is best suited for medium-scale voltages, future development may also incorporate low- and high-scale voltage applications.

References

1.Erickson R. W., Maksimović D. (2001). Fundamentals of Power Electronics, 2nd. Edition. Kluwer Academic Publishers.

2.Tianyang, Junming Z., Xinke W., Kuang S., Youshen W. (2015). A bidirectional LLC resonant converter with automatic forward and backward mode transition. IEEE Trans. Power Electron., vol. 30(2), 757–770.

3.Xia B., Ruan X., Chen W. (2009). Analysis and design of LCC re-sonant converter for high voltage and high-power applications. Transactions of China Electrotechnical Society, 24(5), 60-66.

4.El Khateb,A., Rahim, N., Selvaraj J., Williams B,. (2015). DC-DC converter with low input current ripple for maximum photovoltaic power extraction. IEEE Trans. Ind. Electron., 62(4), 2246-2256.

5.Wang Y., Xue L., Wang C., Wang P., Li W., (2016). Interleaved high conversion-ratio bidirectional DC–DC converter for distributed energy-storage systems—circuit generation, analysis, and design, IEEE Transactions on Power Electronics. 31(8), pp. 5547-5561.

6.Riaz, M., Yasin, A.R., Arshad Uppal, A., & Yasin, A. (2021). A novel dynamic integral sliding mode control for power electronic converters. Science Progress, 104.

7.Tingting H., Lili, Jiangguo Z., (2016). A novel model predictive sliding mode control for AC/DC converters with output voltage and load resistance variations. IEEE Energy Conversion Congress and Exposition (ECCE), 1-6.

8.Malesani L., Rossetto L., Spiazzi G., Tenti P. (1995). Performance optimization of Cuk converters by sliding-mode control. IEEE Transaction on Power Electronics, 10 (3), 302-309.

9.Cucuzzella M. (2015). Design of robust higher order sliding mode control for micro grids. IEEE Journal on Emerging and Selected Topics in Circuits and Systems, 5 (3), 393-401.

10.Schutten M., Torrey D. (2003). Improved small-signal analysis for the phase-shifted PWM power converter. IEEE Trans Power Electron 18(2), 659–669.

11.Ying F., Halivor J., (2019). Sliding mode control of the LCC series-parallel resonant converter (Master's Thesis). College of Automation, Science & Engineering, South China University of Technology, China.

12.Jeronimo J. (2015). Development and implementation of a supervisor strategy and sliding mode control setup for fuel-cell-based hybrid generation systems. IEEE Transactions on Energy Conversion, 30 (1), pp.218-225.

13.Tan, X., Ruan, X., (2016). Equivalence relations of resonant tanks: a new perspective for selection and design of resonant converters. IEEE Trans. Ind. Electron, 63(4), pp. 2111–2123.

14.Abdelhédi, F., & Derbel, N. (2019). On the renovation and analysis of high order sliding mode approaches with application to robotic systems. Int. J. Model. Identif. Control., 31, 374-381.

15.Castilla, M., Garcia de Vicuña, L., Lopez, M., (1997). A sliding mode controller for the current-source parallel-resonant converter with zero-voltage switching. Proc. IEEE IECON, New Orleans, LA, pp. 477–482.

16.Feng X., Tao Y., Cui X., Shao K., Wang Y., (2020). Sliding and predictive current control strategy of the three-phase Vienna rectifier. Journal of Power Electronics, 20(3) 743-753.

17.Dai P., Shi C., Zhang L., Zhang J., (2018). Analysis of synchronous rectification discontinuous PWM for SiC MOSFET three phase inverters. Journal of Power Electronics, 18(5), 1336-1346.

18.Zad, H.S., Ulasyar, A., & Zohaib, A. (2018). Robust Sliding Mode Voltage Control of Three-phase Power System Converter. 2018 International Symposium on Recent Advances in Electrical Engineering (RAEE), 1-5.

19.Ding, Y., Yan, X., Mao, Z., Spurgeon, S.K., & Jiang, B. (2022). System structure based decentralized sliding mode output tracking control for nonlinear interconnected systems. International Journal of Robust and Nonlinear Control, 33, 1704 - 1719.

20.Fang, M., Shi, P., & Dong, S. (2021). Sliding Mode Control for Markov Jump Systems with Delays via Asynchronous Approach. IEEE Transactions on Systems, Man, and Cybernetics: Systems, 51, 2916-2925.

21.Duranay, Z.B., Guldemir, H., & Tuncer, S. (2018). Fuzzy Sliding Mode Control of DC-DC Boost Converter. Engineering, Technology & Applied Science Research.
22.Dong, D. (2009). Modeling and Control Design of a Bidirectional PWM Converter for Single-phase Energy Systems.
23.Alam, M., Eberle, W., Gautam, D.S., & Botting, C. (2017). A Soft-Switching Bridgeless AC–DC Power Factor Correction Converter. IEEE Transactions on Power Electronics, 32, 7716-7726.